CEAS-GNC-2024-027

EuroGNC Navigation Guidance Control CEAS Bristol, UK June 11th-13th 2024
University of BRISTOL ROYAL AERONAUTICAL SOCIETY AIAA

Improving satellite inertia identification with an observability-based EKF

Hélène Evain Control specialist, CNES, 31000 Toulouse, France. helene.evain@cnes.fr

Stéphanie Delavault Estimation expert, CNES, 31000 Toulouse, France. stephanie.delavault@cnes.fr

ABSTRACT

In this paper, the problem of identifying the inertia matrix of a satellite when the input data can be of low observability is tackled. The confidence in the final estimation is of high importance and is harder to assess when a high observability is not guaranteed on every part of the whole dataset. This paper proposes a method that enhances the knowledge of the reliability of the identification process. An extended Kalman filter with variable covariance is implemented and tested with high-fidelity simulator data.

Keywords: Identification, Inertia, Satellite attitude control

Nomenclature

$\mathbf{0}$	=	null vector
I_d	=	identity matrix
diag	=	a diagonal matrix
$\omega = (\omega_x, \omega_y, \omega_z)$	=	angular velocity of the satellite in the satellite reference frame
$\dot{\omega} = (\dot{\omega}_x, \dot{\omega}_y, \dot{\omega}_z)$	=	angular acceleration of the satellite in the satellite reference frame
I_{CB}	=	inertia matrix of the central body of the satellite
I_{SP}	=	inertia matrix of the solar panel of the satellite
h_{tot}	=	total angular momentum of the satellite
h_{RW}	=	sum of the reaction wheels angular momentum
$\dot{h}_{RW}$	=	sum of the reaction wheels torques
$\bar{x}$	=	estimated state of the EKF
$\hat{x}$	=	predicted state of the EKF
$\underline{x}$	=	measured state of the EKF
$\mathbf{u}$	=	input of the EKF
$\mathbf{f}$	=	prediction function of the EKF
$\mathbf{h}$	=	measurement function of the EKF
dt	=	timestep
$\mathbf{P}$	=	covariance matrix of the states in the EKF
$\mathbf{Q}$	=	covariance matrix associated with the prediction equations in the EKF
$\mathbf{R}$	=	covariance matrix associated with the measurement equations in the EKF
$\mathbf{F}$	=	$\mathbf{f}$ state derivative matrix
$\mathbf{H}$	=	$\mathbf{h}$ state derivative matrix
$\mathbf{O}$	=	observability matrix

$\boldsymbol{\Psi}$	=	regressor matrix
M	=	number of states in the EKF

The vectors are in bold lower case and the matrices in bold upper case.

1 Introduction

For demanding satellite attitude control systems, the identification of the inertia matrix is of high importance as its knowledge impacts the agility and pointing performance. Indeed, as explained in Ref. [1, 2], the CNES Microcarb satellite for instance has an attitude control law that directly depends on the known inertia diagonal terms. Even if the robustness is ensured on a large uncertainty set, the performance will be impacted if the true value is far from the known inertia value. In addition, the inertia matrix is always uncertain before flight because on-ground calibrations are difficult, and the inertia values varies with time because of the fuel consumption so there is a legitimate interest to calibrate the inertia value when the satellite is in orbit. In this paper, it is considered that the inertia identification is not calculated on board the satellite but from telemetry data on ground which can limit the available data.

Classical on-ground inertia identification techniques include the least-squares method as described in Ref. [3]. Refinement has been proposed in Ref. [4] where constraints on the positivity are enforced. Other types of methods include the extended Kalman filter (EKF) like in Ref. [5, 6] where the attitude and angular velocity are also estimated. The unscented Kalman filter (UKF) has also proven to be an adequate candidate for identifying the inertia matrix like in Ref. [2, 7, 8]. In Ref. [9], maximum likelihood methods have been studied for inertia identification using telemetry data. Also, the Instrumental Variable (IV) method has proven to be efficient and theoretically unbiased contrary to other methods in Ref. [10, 11] in case of a closed-loop system. Recent improvements have been made to include delay and actuator misalignment in the identification method in Ref. [12], applied to the Microcarb case.

In order to obtain a precise identification with an acceptable confidence level, estimation methods need to have inputs of a minimum observability level. However, this requires the satellite to perform specific maneuvers, imposing operational constraints. There is therefore a need to be able to identify the inertia matrix on data available –usually attitude maneuvers not designed for this purpose. The issue faced here is the observability of the data available for the inertia estimation and the confidence obtained in the identification process. Referred to as experiment design, works of Ref. [13, 14] give interesting observability criteria that became metrics for our previous work Ref. [2]. In Ref. [15], the experiment design is carried out thanks to a cubic spline parametrization and cost functions based on the observability metrics.

In previous related papers Ref. [2, 10–12], the identification methods -consisting in the IV development and validation mainly, and of an UKF - have been designed and their performance evaluated on data with good observability. Then, Ref. [15] tackled the issue of experiment design and Ref. [2] focused on the observability problem and proposed a methodology to select the most observable data to perform the identification, with a comparison between various observability metrics. Divisions into small groups and combinations of the data are proposed and evaluated. This method proved to be efficient but requires a sharp knowledge of the acceptable optimality criteria values. Also, a specific normalization has to be performed with respect to the duration of the maneuvers, and many simulations are necessary to ensure the range of confidence depending on the values of the criteria. Therefore, it requires expert knowledge to run this functionality, and the confidence in the final estimation value is more uncertain especially for the UKF, while the IV remained at very good performance levels.

A need was therefore identified for a simpler method that could give good performance and a reliable confidence level in the output identification especially when the observability is not constant over the dataset. Furthermore, having another identification method in addition to the IV and UKF is precious as

it helps validate the identification results. That is why an extended Kalman filter has been designed and tested, and is the core of this paper. In order to obtain reliable variance on the estimate, the covariance matrices are varying depending on the observability, which is a similar approach to the one proposed in Ref. [16]. It is especially interesting since it enables the identification to focus the evaluation of the interesting data in an autonomous manner, without having to proceed to a thorough evaluation of the data as in Ref. [2]. In addition, tuning the EKF becomes easier and closer to the physical parameters than without this observability dependence. This makes the tool easy to use and generic for different missions and for non-expert engineers, where only a few parameters need to be tuned.

This paper is organized as follow. The first part is devoted to the description of the Microcarb satellite test case as it implies specific derivation of the dynamic equations compared to usual implementations. Then, the extended Kalman filter tested is presented. In the following part, an observability study of the data used for the study and the subsequent explanation of the tuning of the EKF parameters are shown. Finally, the identification results are presented. The paper finishes with a conclusion and perspectives.

2 The Microcarb satellite

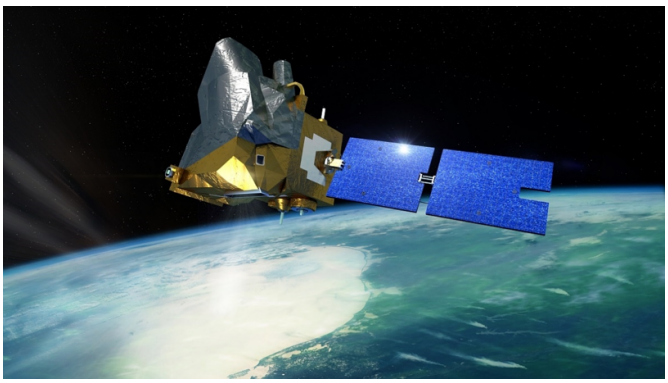

Fig. 1 Microcarb satellite. Credits CNES

Microcarb is a CNES mission dedicated to the study of the CO_2 fluxes in the atmosphere. It intends to lead the way towards the development of a future operational system able to monitor the CO_2 emissions as described in Ref. [17]. A view of the satellite can be seen in Fig. 1. The attitude and orbit control system is based on the CNES AOCS Myriad series of microsatellites described in Ref. [18] with specificities and details provided in Ref. [19]. The identification of the inertia matrix is necessary for the performance of the mission. The sensor in this normal mode is a star tracker. A Kalman filter estimates in real-time the angular velocity and the attitude of the satellite. The reaction wheels ensure the guidance reference tracking, and magnetotorquers counter the external disturbances coming from the space environment and avoid reaction wheel saturation. Many guidance modes exist that require agility on the satellite. Therefore, there can be a variety of excitations along the principal axes of the satellite. Another specific point on Microcarb is that there is a rotating solar panel which inertia is well-known but not negligible compared to the inertia of the main body. The inertia of the solar panel is much less uncertain as it can be measured on-ground contrary to the platform inertia. The orientation of the solar panel with respect to the central body of the satellite varies but is known at each time step. In usual identification methods, only the whole inertia matrix is calculated. An update of the equations used in the identification methods has been carried out in Ref. [2]. The total inertia matrix is divided into two terms and is expressed at the center of gravity of the satellite:

1) the inertia matrix of the solar panel assumed as an input and known;
2) the inertia of the central body that is constant and is to be estimated.

To do the identification simply, it is necessary to assume that the center of gravity is at a constant location on the satellite, and this approximation has been verified as acceptable. A high-fidelity simulator of the Microcarb dynamic behavior in closed-loop, including equipment high-fidelity representation with realistic noises and non-linearity behaviors, has been developed and validated at CNES. For our identification method, the output available by our simulator which are representative of the flight data available on-ground consists of the raw attitude from the star tracker, the estimated attitude and angular velocity of the satellite, the commanded torques and angular momentum of the reaction wheels and the orientation of the solar panel. The simulations are carried out with typical noises and uncertainties.

3 The extended Kalman filter implemented

The justification of the choice of the equations and simplifications are given in subsection 3.3.

3.1 Prediction equations

In this paper, a classical extended Kalman filter has been implemented with variable covariance matrices in discrete time. The estimation states $\hat{\boldsymbol{x}}$ chosen are the total angular momentum of the satellite $\boldsymbol{h_{tot}}$ and the six inertia parameters corresponding to the three diagonal terms $\boldsymbol{I_{xx}}$,$\boldsymbol{I_{yy}}$ and $\boldsymbol{I_{zz}}$ and three off-diagonal terms $\boldsymbol{I_{xy}}$,$\boldsymbol{I_{xz}}$ and $\boldsymbol{I_{yz}}$ of the central body inertia matrix. The choice of the total angular momentum as a state is motivated by the fact that the state transition matrix of the prediction equations is simpler to assess without impacting the quality of the results (see section 3.3). Using the classical dynamic equations of motion in rotation in the satellite reference frame, the prediction equations (1) are given at a time step $k+1$. The input $\mathbf{u}$ is therefore composed of $\boldsymbol{\omega}$, $\dot{\boldsymbol{\omega}}$, $\boldsymbol{h_{RW}}$ and $\dot{\boldsymbol{h}}_{\boldsymbol{RW}}$.

$$\bar{\boldsymbol{x}}(k+1) = \mathbf{f}(\hat{\boldsymbol{x}}(k), \mathbf{u}) = \begin{cases} \bar{\boldsymbol{h}}(k+1) = \hat{\boldsymbol{h}}_{\boldsymbol{tot}}(k) + \\ \qquad + \mathrm{dt}\left((\hat{\boldsymbol{I}}_{\boldsymbol{CB}}(k) + \boldsymbol{I_{SP}})\dot{\boldsymbol{\omega}} + \dot{\boldsymbol{h}}_{\boldsymbol{RW}} + \left((\hat{\boldsymbol{I}}_{\boldsymbol{CB}}(k) + \boldsymbol{I_{SP}})\boldsymbol{\omega} + \boldsymbol{h_{RW}}\right) \times \boldsymbol{\omega}\right) \\ \bar{\boldsymbol{I}}_{\boldsymbol{CB}}(k+1) = \hat{\boldsymbol{I}}_{\boldsymbol{CB}}(k) \end{cases} \tag{1}$$

The state transition matrix which is the partial differentiation of equation (1) with respect to the states is given in equation (2). The cross-product of equation (1) is neglected since its values are orders of magnitudes lower than the other terms.

$$\mathbf{F} = \frac{\partial \mathbf{f}}{\partial \hat{\boldsymbol{x}}} = \begin{bmatrix} 1 & 0 & 0 & \mathrm{dt}\,\dot{\omega}_x & 0 & 0 & \mathrm{dt}\,\dot{\omega}_y & \mathrm{dt}\,\dot{\omega}_z & 0 \\ 0 & 1 & 0 & 0 & \mathrm{dt}\,\dot{\omega}_y & 0 & \mathrm{dt}\,\dot{\omega}_x & 0 & \mathrm{dt}\,\dot{\omega}_z \\ \vdots & 0 & 1 & 0 & 0 & \mathrm{dt}\,\dot{\omega}_z & 0 & \mathrm{dt}\,\dot{\omega}_x & \mathrm{dt}\,\dot{\omega}_y \\ & 0 & 0 & 1 & 0 & 0 & 0 & 0 & 0 \\ & & & & \ddots & & & & \\ 0 & & & \dots & & & & 0 & 1 \end{bmatrix} \tag{2}$$

3.2 Measurement equations

For the measurement equations, it is simply the equation (3).

$$\underline{\boldsymbol{h_{tot}}} = \mathbf{0} \tag{3}$$

The differentiation of equation (3) gives the matrix $\mathbf{H}$ expressed in equation (4).

$$\underline{\boldsymbol{h_{tot}}} = \frac{\partial \mathbf{h}}{\partial \hat{\boldsymbol{x}}} = \begin{bmatrix} 1 & 0 & 0 & 0 & \dots & 0 \\ 0 & 1 & 0 & 0 & \dots & 0 \\ 0 & 0 & 1 & 0 & \dots & 0 \end{bmatrix} \tag{4}$$

3.3 Justification of the approximations

As can be deduced from the choice of the equations, the external torques are neglected as well as the magnetotorquer action and this is because the data that will confer observability and more precise identification results is located in agile maneuvers where the external torques are negligible. In order to ensure a precise estimation, this study proposes to vary the diagonal terms of $\mathbf{Q}$ and in particular the terms related to the prediction of the total angular momentum. When the observability is high enough, this covariance becomes very small so that the innovations calculated in the Kalman filter are associated with the inertia updates and not the total angular momentum which remains constant enough at the timescale of an attitude maneuver. Indeed, if there is a discrepancy in the estimation process during agile maneuvers, the inertia should be updated and not the total angular momentum from a physical point of view, as there is no other major contributor of external disturbance during the maneuvers for this type of satellite. Like this, the convergence of the inertia states of the EKF can be very fast when there is enough observability. The covariance matrix of the estimates follows the observability trend. Indeed, as seen in Ref. [2], for the UKF, when maneuvers are followed by guidance modes where there is no agility, the disturbances, noise and other non-linear effects that cannot be modeled through the identification method become predominant and impact the identification performance since the algorithm may correct the inertia to match the data during the calm period. From an observability point of view, having the maneuvers plus the calm guidance period will not decrease the observability level of the whole dataset since the necessary information is present so data that does not confer observability and can decrease the precision of the estimation is not detectable. This is why this approach of modifying the covariance matrix is chosen, to help the algorithm correct the right parameters depending on the satellite movement.

4 EKF observability and tuning

4.1 Observability analysis

For this paper, a set of maneuvers representing a typical day of the Microcarb mission is used. The set of simulated maneuvers is shown below in Fig. 2.

In this typical day, it can be noticed that the Y-axis of the satellite is much more solicited than the other axes and especially more than the X-axis. On the X-axis, there is only one major maneuver at around 31 000s. For this paper, the study is considered between 300 seconds and 60 000s including therefore the maneuver soliciting the satellite X-axis. From Ref. [20], the uniform observability condition of the EKF can be checked by ensuring bounds on the observability matrix which is given with the formula in equation (5), by extension of the linear case to the non-linear system studied in the EKF.

$$\mathbf{O}(k-M,k) = \begin{bmatrix} \mathbf{H}(k-M) \\ \mathbf{H}(k-M+1)\mathbf{F}(k-M) \\ \vdots \\ \mathbf{H}(k)\mathbf{F}(k-1)\dots\mathbf{F}(k-M) \end{bmatrix} \tag{5}$$

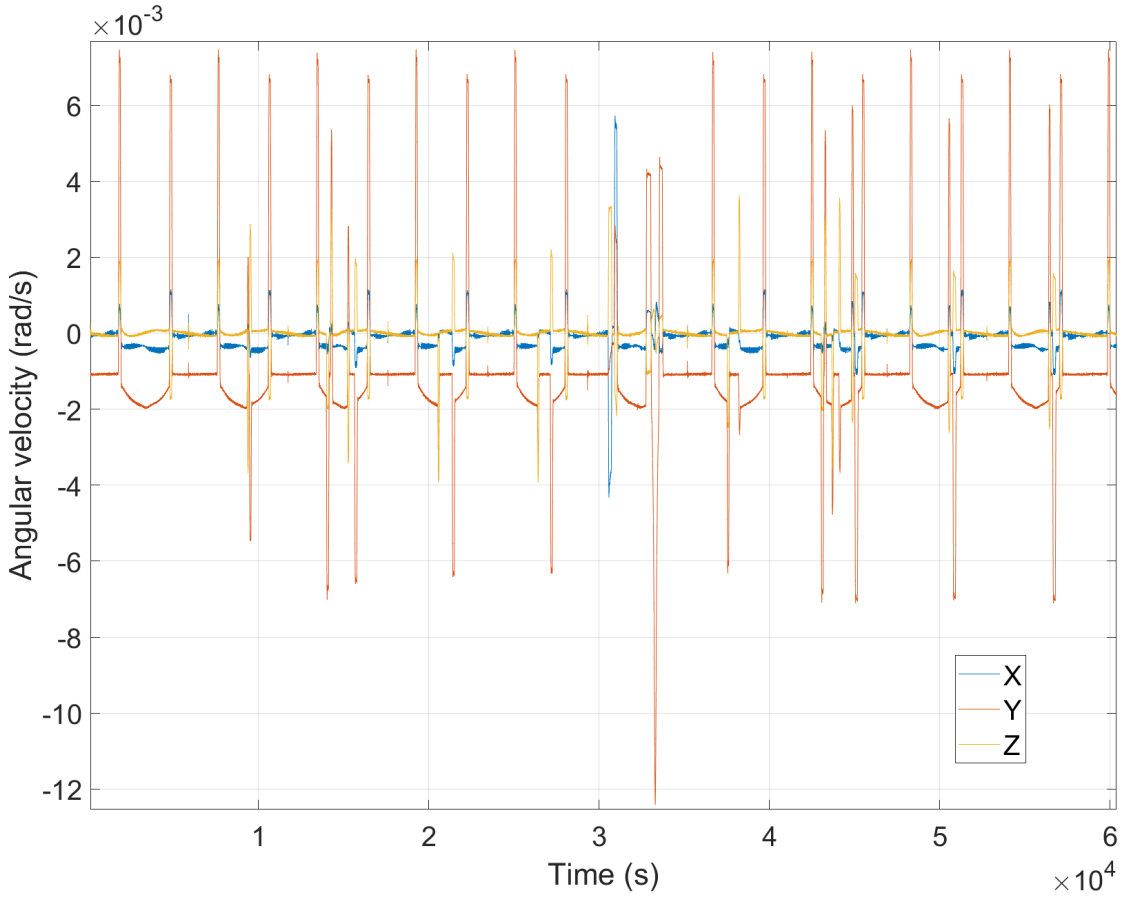

Fig. 2 Typical day of Microcarb – dataset used for this analysis

The lowest singular value of $\mathbf{O}(k-M,k)$ is then calculated. Indeed, even if the rank of the matrix shows that the EKF is uniformly stable, it could be due to the noise that prevents the singular value from being exactly zero. On this dataset, the observed minimal value of the observability matrix is given in Fig. 3 along with the angular velocity profile associated.

The observability condition is always verified since the minimal singular value is of 6e-9 (ensuring the condition of Ref. [20]) but the singular values are much higher when maneuvers take place, which is logical given that the $\mathbf{F}$ matrix depends mainly on the angular accelerations. Then, a local observability measure is chosen for tuning the varying covariance, inspired by the work of Ref. [13, 14], and the evaluation of Ref. [2] which considered the E-optimality criterion as the most efficient metrics. At each time step, the regressor matrix $\mathbf{\Psi}$ is calculated like defined in equation (6).

$$\mathbf{\Psi} = \begin{bmatrix} \dot{\omega}_x & 0 & 0 & \dot{\omega}_y & \dot{\omega}_z & 0 \\ 0 & \dot{\omega}_y & 0 & \dot{\omega}_x & 0 & \dot{\omega}_z \\ 0 & 0 & \dot{\omega}_z & 0 & \dot{\omega}_x & \dot{\omega}_y \end{bmatrix} \tag{6}$$

The vector $\boldsymbol{\xi}$ is deduced with equation (7). It represents the local observability for each of the three axes of the satellite.

$$\boldsymbol{\xi} = \begin{bmatrix} \mathbf{\Psi}(:,1)\mathbf{\Psi}(:,1)^T \\ \mathbf{\Psi}(:,2)\mathbf{\Psi}(:,2)^T \\ \mathbf{\Psi}(:,3)\mathbf{\Psi}(:,3)^T \end{bmatrix} \tag{7}$$

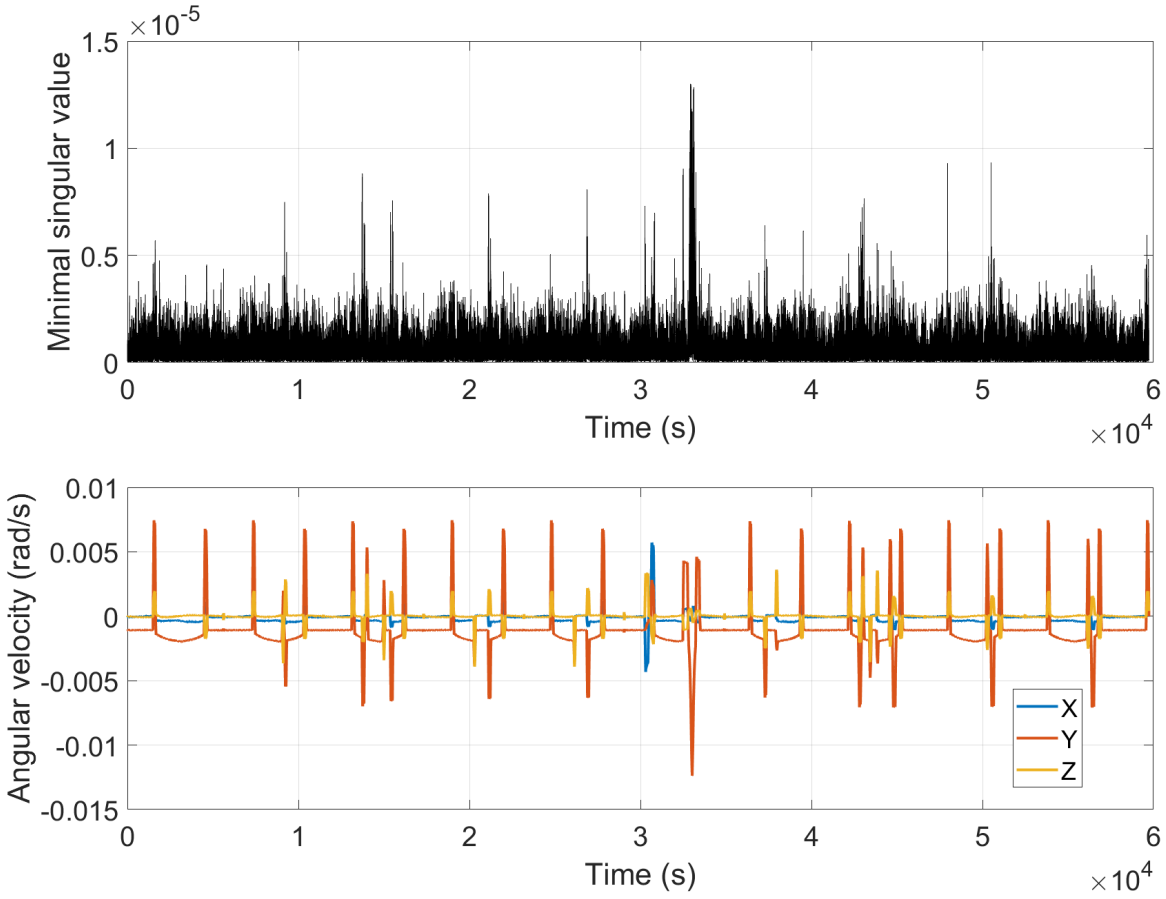

Fig. 3 Minimal singular value of the observability matrix of the EKF (upper subfigure). Angular velocity along each satellite axis (lower subfigure)

For each axis, if the obtained value is higher than a defined threshold, then the associated covariance term is replaced by a lower value in the covariance matrix $\mathbf{Q}$ associated with the total angular momentum equations. On the presented dataset, Fig. 4 shows the values obtained with these calculations.

These values are consistent with the angular velocities. A threshold of $\tau = 0.3.10^{-8}$ is chosen given the results of Fig. 4 to keep an acceptable observability level and filter noisy data.

4.2 Tuning of the EKF with variable covariance

The covariance matrix $\mathbf{Q}$ is given in equation (8).

$$\mathbf{Q} = \begin{bmatrix} \boldsymbol{Q_1} & \mathbf{0_{3x6}} \\ \mathbf{0_{6x3}} & \boldsymbol{Q_2} \end{bmatrix} = \begin{bmatrix} \alpha_1 & 0 & 0 & 0 & 0 & 0 & 0 & 0 & 0 \\ 0 & \alpha_2 & 0 & 0 & 0 & 0 & 0 & 0 & 0 \\ 0 & 0 & \alpha_3 & 0 & 0 & 0 & 0 & 0 & 0 \\ 0 & 0 & 0 & 10^{-6} & 0 & 0 & 0 & 0 & 0 \\ 0 & 0 & 0 & 0 & 10^{-6} & 0 & 0 & 0 & 0 \\ 0 & 0 & 0 & 0 & 0 & 10^{-6} & 0 & 0 & 0 \\ 0 & 0 & 0 & 0 & 0 & 0 & 10^{-7} & 0 & 0 \\ 0 & 0 & 0 & 0 & 0 & 0 & 0 & 10^{-7} & 0 \\ 0 & 0 & 0 & 0 & 0 & 0 & 0 & 0 & 10^{-7} \end{bmatrix} \tag{8}$$

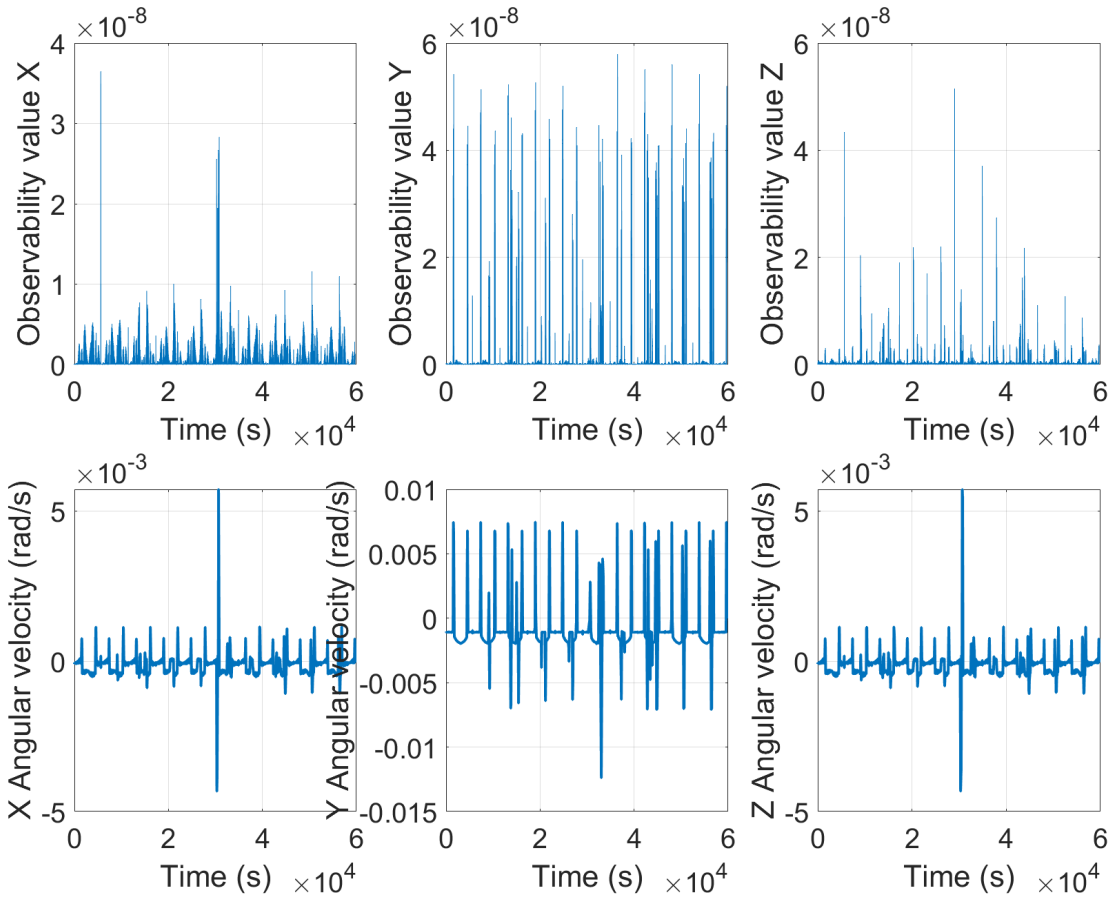

Fig. 4 Observability along time with respect to each axis (upper subfigures). Angular velocity along each satellite axis (lower subfigures)

The value of α_i is given in equation (9).

$$\alpha_i = \begin{cases} 10^{-4}, & \boldsymbol{\xi}(i) \leq \tau \\ 10^{-9}, & \boldsymbol{\xi}(i) > \tau \end{cases}, i = 1 \ldots 3 \tag{9}$$

The first α value has been calculating by taking into account the fact that external torques are neglected and the modelling during calm periods is less representative. For the second value, there is a need to make a significant gap and ensure the ratio with the terms of $\boldsymbol{Q_2}$ is high enough. It is the ratio with $\boldsymbol{Q_1}$ that is of importance for the first three diagonal terms of $\boldsymbol{Q_2}$. These terms are located between the two possible α values. The covariance of the off-diagonal terms of the inertia matrix are given a lower value since these inertia values are known to be small, and thus should remain small in the identification output. For the measurement covariance matrix, $\mathbf{R} = 10^{-4}\boldsymbol{I_d}$ for the same reason as the first possible value of α: the external torques neglected. To conclude, tuning this EKF is rather simple because it takes into account the physical knowledge of the equations in the case where there is no observability. When there is, the ratio between $\boldsymbol{Q_1}$ and $\boldsymbol{Q_2}$ values becomes more important and is to be tuned.

4.3 Tuning of the EKF with fixed covariance

Tuning the variable-covariance EKF has proven to be simpler than the fixed-covariance which required trial and errors to be convergent. As mentioned in Ref. [2], to obtain satisfactory results, it was necessary to choose covariance values far lower than the physical noises of the system for $\boldsymbol{Q_1}$ especially: $\boldsymbol{Q_1} = 10^{-9}\boldsymbol{I_d}$, $\boldsymbol{Q_2} = \mathbf{diag}(10^{-11}, 10^{-11}, 10^{-11}, 10^{-12}, 10^{-12}, 10^{-12})$, $\mathbf{R} = 10^{-5}\boldsymbol{I_d}$.

4.4 Other parameters for the identification

For the simulations presented in the next part, the initial state of the EKF is:

$\hat{\boldsymbol{x}}_{\boldsymbol{0}} = (0, 0, 0, 12.5, 23.7, 18.2, -1, -1, -1)$ which represents 5% error in the diagonal terms of the inertia matrix compared to the true value. These values are coherent with on-ground estimates and uncertainties on the inertia matrix before flight. The initial covariance of the state is: $\boldsymbol{P_0} = \begin{bmatrix} \boldsymbol{I_d} & \boldsymbol{0_{3x3}} & \boldsymbol{0_{3x3}} \\ \boldsymbol{0_{3x3}} & \boldsymbol{I_d} & \boldsymbol{0_{3x3}} \\ \boldsymbol{0_{3x3}} & \boldsymbol{0_{3x3}} & 0.01\boldsymbol{I_d} \end{bmatrix}$

5 Identification results

5.1 Results with the fixed-covariance EKF

The classical EKF is first implemented and the final values of the identification for this case is given in Tab. 1.

Table 1 Identification results for the fixed-covariance EKF case

	True value ($kg.m^2$)	Estimated value ($kg.m^2$)	Relative errors (%)
I_{xx}	13.907	13.435	3.394
I_{yy}	21.625	21.469	0.724
I_{zz}	20.220	19.856	1.801
I_{xy}	-0.821	-0.611	25.574
I_{xz}	-0.847	-0.605	28.670
I_{xy}	-0.331	-0.261	21.346

The final relative error is below 5% for the EKF with the fixed-covariance case for the diagonal terms which are the most important parts. The off-diagonal terms remain small and acceptable even if the relative errors are high. The estimation results with respect to time are given in Fig. 5, 6 and 7. It can be noticed that the identification improves during the maneuvers, especially for the X-axis where only one maneuver is of importance like noticed in Fig. 2.

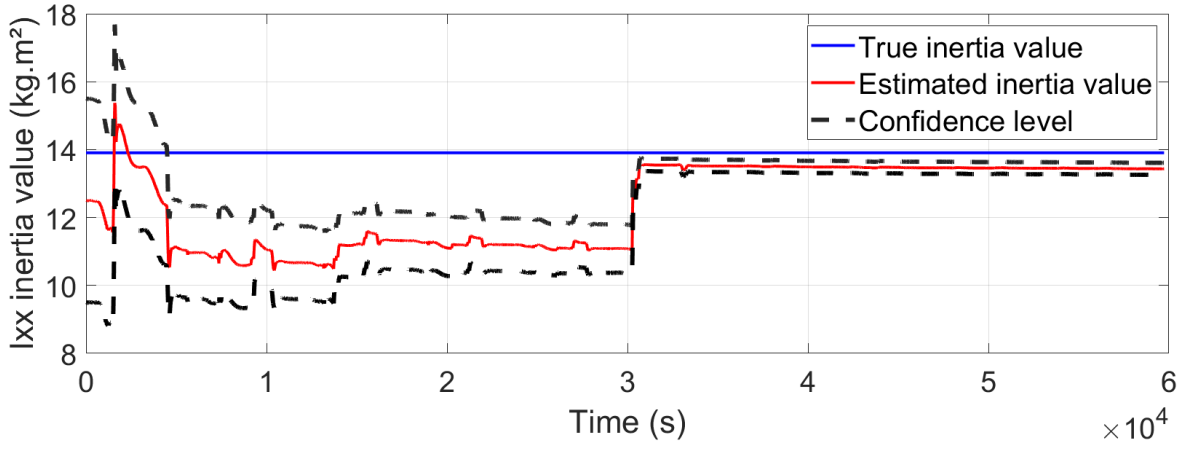

Fig. 5 Result of the identification with respect to time of the EKF with fixed-covariance for the X-axis

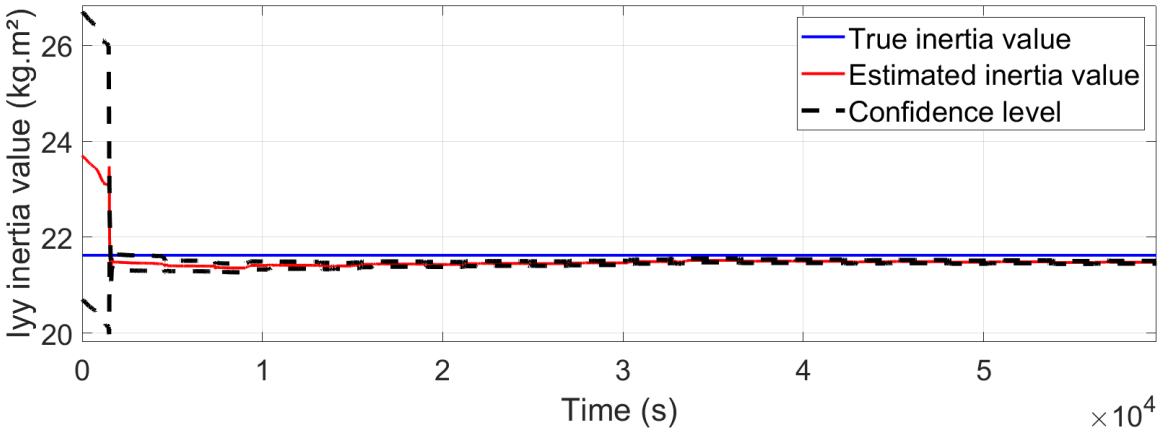

Fig. 6 Result of the identification with respect to time of the EKF with fixed-covariance for the Y-axis

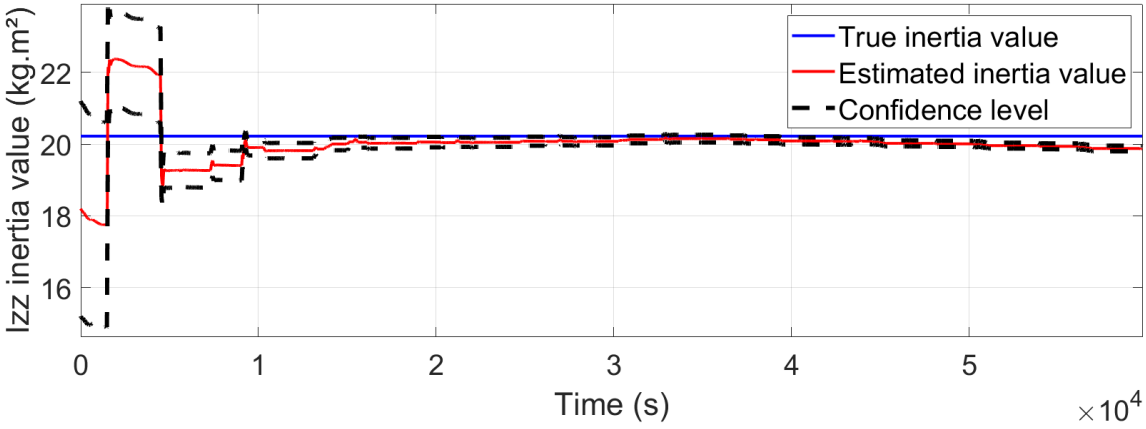

Fig. 7 Result of the identification with respect to time of the EKF with fixed-covariance for the Z-axis

The final results are precise, however the confidence level corresponding to the 3-sigma values issued from the covariance matrix of the estimated states does not include the true value so is not correct and cannot be trusted. That is why a varying covariance has been implemented.

5.2 Results with the varying-covariance EKF

The final values of the identification with a varying-covariance EKF are given in Tab. 2. The final

Table 2 Identification results for the EKF with the varying-covariance case

	True value ($kg.m^2$)	Estimated value ($kg.m^2$)	Relative errors (%)
I_{xx}	13.907	13.630	1.990
I_{yy}	21.625	21.357	1.241
I_{zz}	20.220	20.356	0.673
I_{xy}	-0.821	-0.703	14.379
I_{xz}	-0.847	-0.869	2.535
I_{xy}	-0.331	-0.531	60.272

values are very good with very small errors for the diagonal terms and the off-diagonal ones remain in very acceptable values. However, the main advantage of this method can be seen in Fig. 8, 9 and 10. In this case, the confidence levels follow better the maneuvers and the true value is now located inside

the confidence level. The interval of confidence increases during the phases of low motion. The values given in Tab. 1 and 2 are the final estimates, however it would be interesting to select as output the estimates when the covariance is the lowest, for instance in Fig. 8 in the X-axis, it would be preferable to select the identified value when the covariance is at lowest. The identification results for the covariance vary more rapidly than with the fixed-covariance case when there are maneuvers so when observability is higher, which is the expected behavior. An advantage of this method is therefore to simply launch the identification on the data without doing an observability analysis beforehand. The method takes into account the current observability of the data autonomously. In addition, the covariance level shows directly if the estimate is reliable or not, and for instance, if only the 25 000 seconds of data were available, then the user would know that the I_{xx} value would not be reliable enough, which was less obvious in Fig. 5.

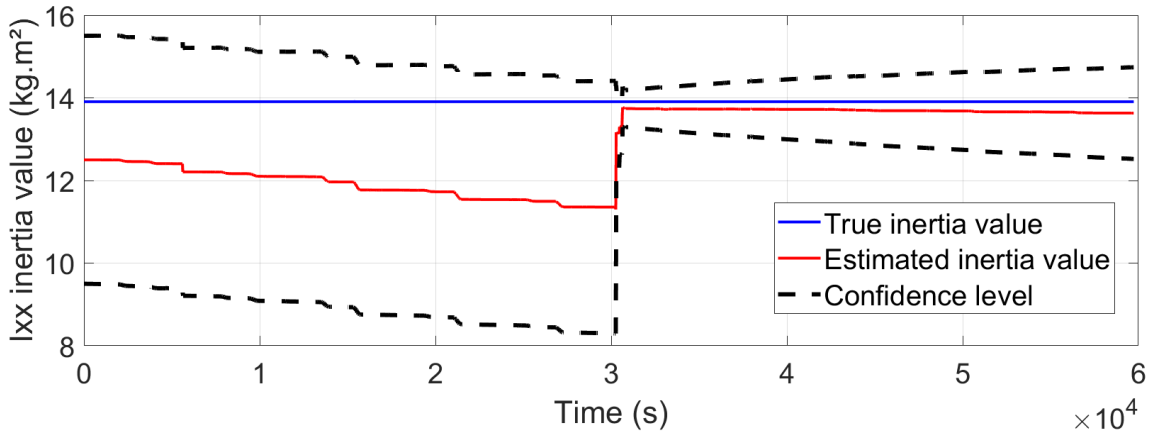

Fig. 8 Result of the identification with respect to time of the EKF with varying-covariance for the X-axis

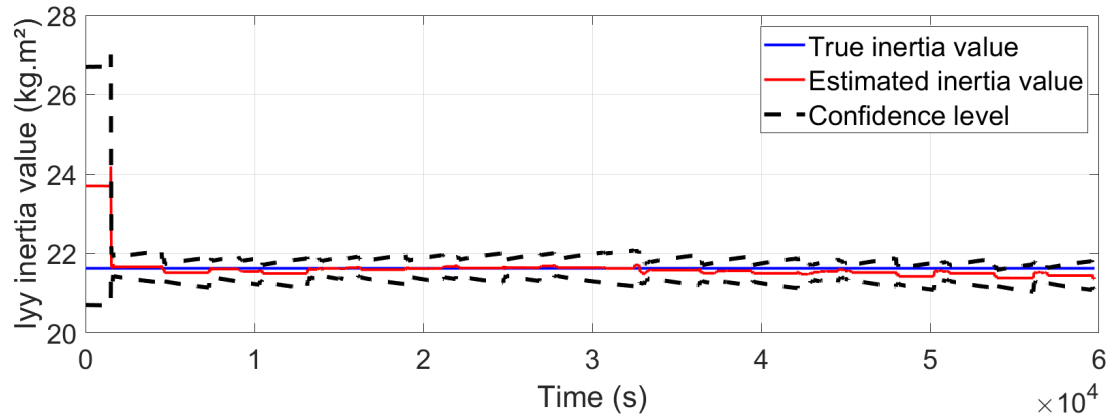

Fig. 9 Result of the identification with respect to time of the EKF with varying-covariance for the Y-axis

6 Conclusion

In this paper, the identification of the inertia matrix problem with observability constraints is first presented and justifies the development of a method that can provide reliable information about the variance of the estimate with respect to time. Indeed, for operational purposes, it is of high importance to be able to assess the reliability of the output, especially with data that can be of mixed-level of observability. Therefore, an extended Kalman filter with variable covariance has been implemented. The values of the estimates are close to the true ones and compared to the EKF with fixed-covariance, the confidence level is more representative of the true performance of the identified estimates. A weighted

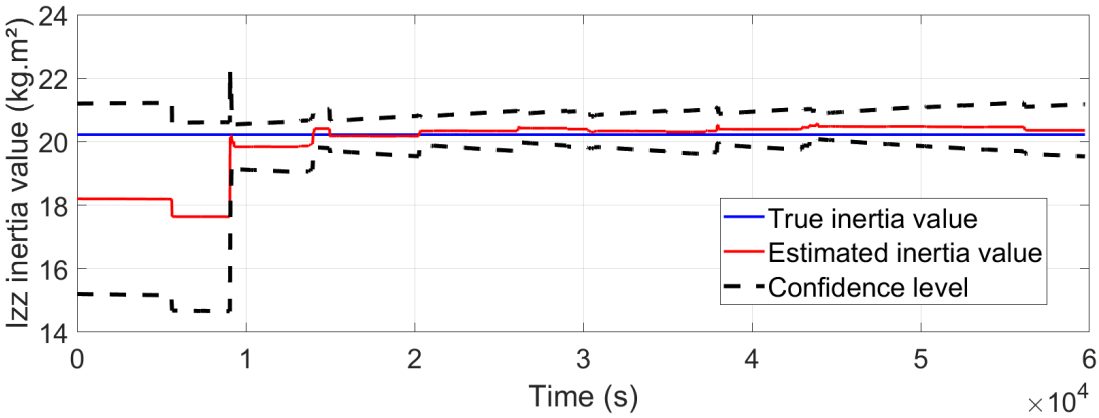

Fig. 10 Result of the identification with respect to time of the EKF with varying-covariance for the Z-axis

IV method has also been implemented, however as long as the observability is of a minimal value, the classical IV method performs very well, especially since it has been tuned precisely for the Microcarb mission. For other missions where the filters would not be perfectly tuned, it could be of interest to implement this type of method where including the observability helps the algorithm to focus on the interesting data. The next step would be to test the methods on telemetry data to compare the results of the estimation for different datasets.

References

[1] F. Genin and F. Viaud. An innovative control law for microcarb microsatellite. In *AAS Conference on Guidance, Navigation and Control*, Breckenridge, USA, Feb. 2018.

[2] G. Magnani, H. Evain, and S. Delavault. Satellite inertia estimation and observability analysis. In *9th European Conference For Aeronautics And Space Sciences (Eucass)*, Breckenridge, USA, July 2022.

[3] A.Y. Lee and J.A. Werte. In-flight estimation of the cassini spacecraft's inertia tensor. *Journal of spacecraft and rockets*, 39(1):153–155, 2002.

[4] Z. R. Manchester and M. A. Peck. Recursive inertia estimation with semidefinite programming. In *Proceedings of the 2017 AIAA Guidance, Navigation, and Control Conference*, 2017.

[5] H. Yoon, K. M. Riesing, and K. Cahoy. Kalman filtering for attitude and parameter estimation of nanosatellites without gyroscopes. *Journal of Guidance, Control and Dynamics*, 40(9):2272–2288, 2017.

[6] A. Bellar and M.A Si Mohammed. Satellite inertia parameters estimation based on extended kalman filter. *J Aerosp Technol Manag*, 11, 2019.

[7] P. Sekhavat, M. Karpenko, and I. Ross. Ukf-based spacecraft parameter estimation using optimal excitation. In *Proceedings of the 2009 AIAA Guidance, Navigation, and Control Conference*, 2009.

[8] A. Kornienko, P. Dhole, R. Geshnizjani, P. Jamparueang, and W. Fichter. Determining spacecraft moment of inertia using in-orbit data. In *10th international ESA conference on Guidance, Navigation and Control Systems*, 2017.

[9] M.L. Psiaki. Estimation of a spacecraft's attitude dynamics parameters by using flight data. *Journal of Guidance, Control and Dynamics*, 28(4):594, 2005.

[10] C. Nainer, H. Garnier, M. Gilson, and C. Pittet. In-orbit data driven identification of satellite inertia matrix. In *Proceedings of the 18th IFAC Symposium on System Identification*, volume 51, page 467–472, 2018.

[11] C. Nainer, H. Garnier, M. Gilson, H. Evain, and C. Pittet. In-flight inertia matrix estimation of a gyroless satellite. In *Proceedings of the 2019 CEAS Specialist Conference on Guidance, Navigation and Control (EuroGNC)*, 2019.

[12] C. Nainer, H. Garnier, M. Gilson, H. Evain, and C. Pittet. Parameter estimation of a gyroless micro-satellite from telemetry data. *Control Engineering Practice*, 123:594, 2022.

[13] G. Franceschini and S. Macchietto. Model-based design of experiments for parameter precision: State of the art. *Chemical Engineering Science*, 63(19):4846–4872, 2008.

[14] L. Walter, É.and Pronzato. Qualitative and quantitative experiment design for phenomenological models - a survey. *Automatica*, 26(2):195–213, 1990.

[15] C. Nainer, H. Garnier, M. Gilson, C. Pittet, and H. Evain. Design of satellite maneuvers for inertia parameter estimation. *Proceedings of the 21st IFAC World Congress*, 53(2):14894–14899, 2020.

[16] J. H. Ramos, D. W. Adams, K. M. Brink, and M. Majji. Observability informed partial-update schmidt kalman filter. In *2021 IEEE 24th International Conference on Information Fusion (FUSION)*, pages 1–8, 2021.

[17] P. et als Veronique. A new space instrumental concept based on dispersive components for the measurement of co2 concentration in the atmosphere. *ICSO*, 2012.

[18] M. Le Du, J. Maureau, and P. Prieur. Myriade: an adaptative aocs concept. In *5th international ESA conference on Guidance, Navigation and Control Systems*, 2005.

[19] G. Rineau, F. Genin, and S. Delavault. Myriade: an adaptative aocs concept. In *11th international ESA conference on Guidance, Navigation and Control Systems*, 2021.

[20] Y. Song and J. W. Grizzle. The extended kalman filter as a local asymptotic observer for discrete-time nonlinear systems. *Journal of Mathematical Systems, Estimation and Control*, 8(1):59–78, 1995.